SUPPORTING MATERIAL

Minimizing the impact of photoswitching of fluorescent proteins on FRAP analysis

Florian Mueller[1,2], Tatsuya Morisaki[1], Davide Mazza and James G. McNally[3]

Laboratory of Receptor Biology and Gene Expression
National Cancer Institute
Bethesda, MD 20892

[1]equal contribution

[2] current address: Institut Pasteur, Imaging and Modeling Group CNRS, URA 2582, F-75015, Paris, France

[3] corresponding author: mcnallyj@exchange.nih.gov

1. Alternate explanations for fluorescence recovery: detector photoblinding and diffusion

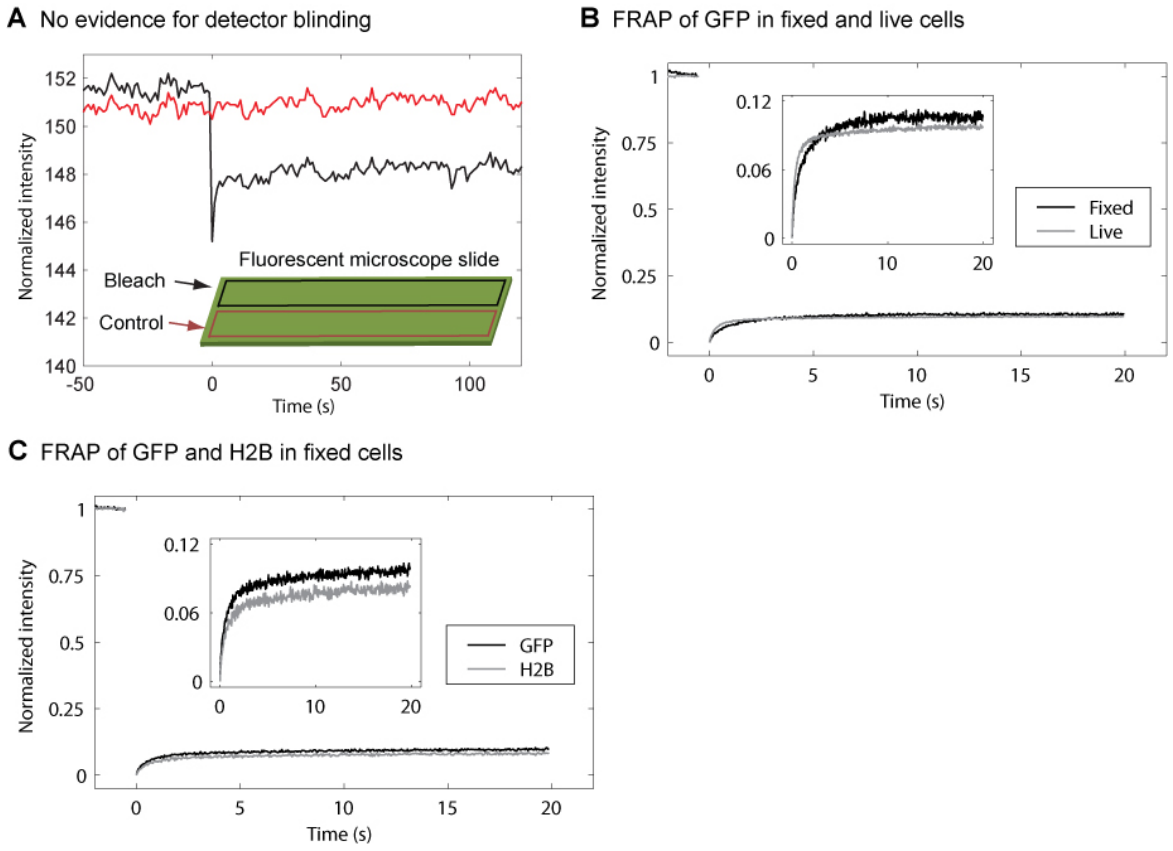

Figure S1. *Testing potential roles for either detector blinding and diffusion in the whole-cell FRAP recoveries. (A) FRAP on a fluorescent plastic slide to test if the detector sensitivity transiently changes after the intentional photobleach (detector blinding (3)). Upper half of the imaged area was photobleached (black rectangle) and intensity was measured in the bleached and the control area underneath (red rectangle). The control curve is flat indicating that the detector has not lost sensitivity after the photobleach, and so detector blinding does not occur and cannot be the cause of the recoveries in the whole-cell photobleach. (B) Whole-cell photobleach performed on live and fixed cells (inset shows a zoomed-in view). Fixed cells show similar recoveries to live cells, indicating that diffusion is not a major cause of the recovery. (C) Whole-cell bleach performed on fixed cells containing either GFP or H2B-GFP (inset shows a zoomed-in view). Bleach depth is renormalized to zero. Fixed GFP yielded only a slightly larger recovery than fixed H2B (9.5% vs. 8.0%). This indicates that most molecules are fixed by the 1 hour fixation procedure. However, the 1.5% difference suggests that this small fraction of GFP molecules remained free after fixation. This allows us to estimate the error introduced by incomplete fixation when using fixed H2B-GFP to estimate reversible fractions for our correction procedure. Without any correction we found that H2B-GFP had at most a 5% free fraction. If only 1.5% of this free fraction escapes fixation, then 1.5% x 5% = 0.08% of the total H2B-GFP molecules will remain free after fixation. This contributes negligibly to our measurement.*

2. Correcting for photoswitching arising from pre-bleach and post-bleach imaging

Two correction procedures can be used to account for the loss of fluorescence due to observational photobleaching. The conventional procedure measures fluorescence during the recovery in a region far away from the photobleach spot, and then normalizes the recovery based on the loss of fluorescence in this distant region. This approach also corrects for the loss of fluorescence due to the intentional photobleach, since these bleached molecules eventually diffuse into the distant measurement region. A more rigorous approach however should correct these two independent events separately. In the approach we advocate, observational photobleaching can be corrected by measuring the fluorescence decay rate at the same location as the bleach spot but after the FRAP recovery has equilibrated. Normalizing the FRAP recovery by this decay rate results in a corrected curve that does not fully recover to one. If the molecule under study does not have an immobile fraction (see Mueller et al. (3) for how to test this independently), then the missing fluorescence must be due to the loss of fluorescence caused by the intentional photobleach, which can be estimated and incorporated into the FRAP model based on the measured profile of the photobleach (3). We have found that this altered procedure gives less variability in the quantitative estimates from FRAP (3), but we do not know how critical this is in the larger context of our new procedure for correction of photoswitching, which may have additional errors in estimating the reversible fraction that exceed those due to the observational photobleaching correction procedure.

When using this alternate procedure for correcting observational photobleaching, we found an additional correction was necessary when FRAP data were generated on two of our Zeiss microscopes. The reason for this correction procedure is described in the figure below, along with the details of this additional correction procedure. The additional correction is not necessary if the FRAP data are corrected for observational photobleaching using the conventional approach.

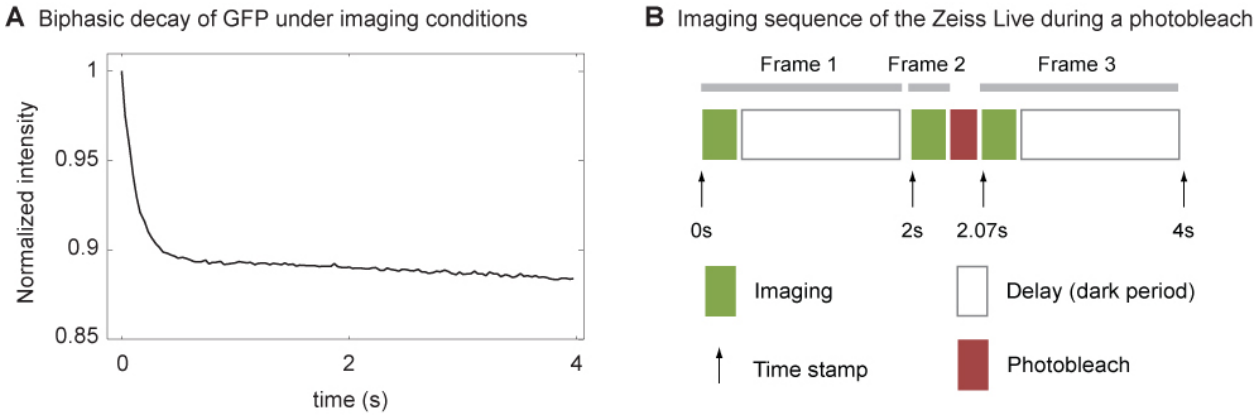

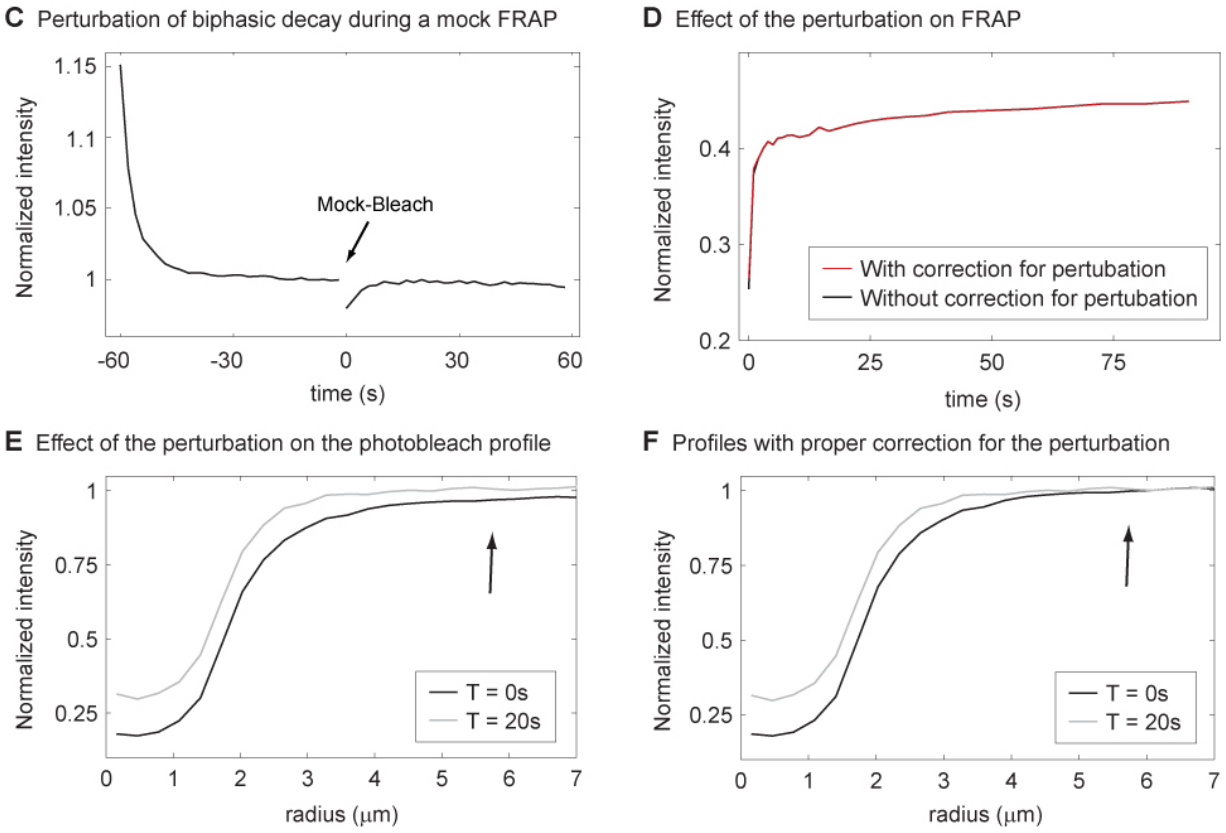

Figure S2. *Effects of photoswitching during the imaging phase of a FRAP experiment. (A) Photoswitching of GFP under imaging conditions. Cells expressing H2B-GFP were imaged for a total of 4 s at an acquisition frequency of 25 Hz. Intensity was measured in the entire nucleus and renormalized to the intensity at t=0 s. The biphasic decay of fluorescence reflects a combination of "reversible" photoswitching and "irreversible" photobleaching (4). (B) Schematic of the FRAP imaging sequence on the Zeiss LSM 5 Live when delays are introduced. The additional image after the FRAP disturbs the equilibrium between photoswitching and photobleaching, and so introduces a perturbation in the decay rate. (C) This perturbation can be detected by performing a FRAP experiment with the photobleach positioned in the medium outside of the cell (a mock FRAP). The average fluorescence intensity measured in the nucleus shows a dip right after the mock photobleach. (D) This small perturbation should be accounted for in the procedure to correct for the loss of fluorescence due to imaging. Most such procedures will automatically correct for the effect since they measure fluorescence from another location in the cell at the same set of time points during the recovery. Our procedure however measures the fluorescence decay from a separate control measurement. Even in this case we found that the correction for the perturbation had a negligible effect on the FRAP curve. (E) The perturbation has a significant effect on the estimate of the photobleach intensity profile measured right after the photobleach (t=0 s). The uncorrected t=0 s profile fails to rise at its edges to the normalized cellular fluorescence of one. This makes it impossible to fit these curves with a plausible, physical model. Later curves (t=20 s) taken after the perturbation has dissipated rise to one at their edges. (F) The perturbation can be corrected by normalizing the image data with the intensity data obtained from a mock FRAP. After incorporating this correction, the t=0 s profile now returns to one at its edges. We suggest therefore that a mock photobleach be performed to test for this effect, and then if found, that it be used to correct the intensity profile of the photobleach used in the FRAP model.*

3. Converting from FRAP to photoactivation (or FLAP)

Here we show how the reaction-diffusion equations for photoactivation (or FLAP) are given by one minus the reaction-diffusion equations for FRAP (i.e. $FLAP = 1 - FRAP$). This is useful for constructing a solution for photoswitched molecules. It also demonstrates that FRAP and FLAP are mathematically equivalent. The latter result argues against the intuitive expectation that FLAP is better at estimating off rates than FRAP.

We assume two forms of molecules, those that are free (f) and those that are bound (c) to an immobile substrate. We also presume that f and c have reached their equilibrium values F_{eq} and C_{eq} across the cell, and that the total concentration has been normalized to one: $F_{eq} + C_{eq} = 1$. The argument below is independent of the details of the spatial dependence of the FRAP, but for simplicity, we will assume that there is radial symmetry, and so $f = f(r,t)$ and $c = c(r,t)$ (3).

Both FRAP and FLAP detect the changes in f and c, so all experiments are subject to the same set of equations describing the diffusion and binding of the fluorescent molecules (5):

$$\begin{aligned} \frac{\partial f}{\partial t} &= D_f \nabla^2 f - k_{on}^* f + k_{off} c \\ \frac{\partial c}{\partial t} &= k_{on}^* f - k_{off} c \end{aligned} \qquad 3.1$$

Moreover, the initial conditions for FRAP and FLAP are also described by the same type of equation

$$f(r,0) = F_{eq} \times P(r), \quad c(r,0) = C_{eq} \times P(r) \qquad 3.2$$

where P corresponds to either the photobleaching or the photoactivation profile. Note that these profiles are the only difference between FRAP and FLAP. The FRAP profile (P_{ble}) is concave upward reflecting a reduction in fluorescence in the bleach zone, whereas the FLAP profile (P_{act}) is concave downward reflecting an activation of fluorescence in the activation zone (see Fig. S3).

Let f_{ble} and c_{ble} be the fluorescence concentrations in a FRAP experiment produced by the photobleach profile P_{ble}, and let f_{act} and c_{act} be the fluorescence concentrations in a FLAP experiment produced by the photoactivation profile P_{act}. Then the initial conditions Eq. 3.2 can be rewritten for these two cases:

$$f_{ble}(r,0) = F_{eq} \times P_{ble}(r), \quad c_{ble}(r,0) = C_{eq} \times P_{ble}(r) \qquad 3.3$$

$$f_{act}(r,0) = F_{eq} \times P_{act}(r), \quad c_{act}(r,0) = C_{eq} \times P_{act}(r) \qquad 3.4$$

To see how these initial conditions P_{ble} and P_{act} are connected, we make the change of variables

$$u_{ble}(r,t) = F_{eq} - f_{ble}(r,t) \qquad \text{and} \qquad v_{ble}(r,t) = C_{eq} - c_{ble}(r,t). \tag{3.5}$$

The new variables, u_{ble} and v_{ble}, also satisfy the reaction diffusion equations 3.1, as can be shown by simple substitution. The initial conditions for the new variables can be obtained by substituting Eq. 3.3 into Eq. 3.5 yielding:

$$u_{ble}(r,0) = F_{eq}(1-P_{ble}) \qquad v_{ble}(r,0) = C_{eq}(1-P_{ble}). \tag{3.6}$$

Note that the term $1-P_{ble}$ inverts the photobleach profile so that this term yields a concave downward function corresponding to a photoactivation profile (Fig. S3). Specifically, if

$$P_{act} = 1-P_{ble} \tag{3.7}$$

then Eq. 3.6 is identical to Eq. 3.4, and so we have converted the FRAP variables into the photoactivation variables by Eq. 3.5. Thus, when $P_{act} = 1-P_{ble}$, we have:

$$f_{act} = u_{ble} \qquad c_{act} = v_{ble}. \tag{3.8}$$

Substitution of Eq. 3.8 into Eq. 3.5 yields:

$$f_{act}(r,t) = F_{eq} - f_{ble}(r,t) \qquad \text{and} \qquad c_{act}(r,t) = C_{eq} - c_{ble}(r,t). \tag{3.9}$$

Since both FRAP and FLAP are given by the sum of their respective free and bound concentrations of fluorescent molecules we have:

$$FLAP = f_{act} + c_{act} = \left(F_{eq} - f_{ble}\right) + \left(C_{eq} - c_{ble}\right) = F_{eq} + C_{eq} - (f_{ble} + c_{ble}) = 1 - FRAP. \tag{3.10}$$

Figure S3. *Relationship between the initial intensity profiles of FRAP and FLAP. The intensity profile of FRAP ($P_{ble}(r)$) was calculated with*

$$P_{ble}(r) = \begin{cases} \theta & \text{for } r \le r_c \\ 1-(1-\theta)\exp\left(-\dfrac{(r-r_c)^2}{2\sigma^2}\right) & \text{for } r > r_c, \end{cases}$$

where $\theta = 0.2$ is the depth of the bleach, $\sigma = 1\mu m$ is the width of the Gaussian and $P_{ble}(r)$ $r_c = 1\mu m$ is the radius of the constant portion (see Appendix 2 in (3)) . The corresponding photoactivation profile was then calculated as $P_{act} = 1-P_{ble}(r)$.

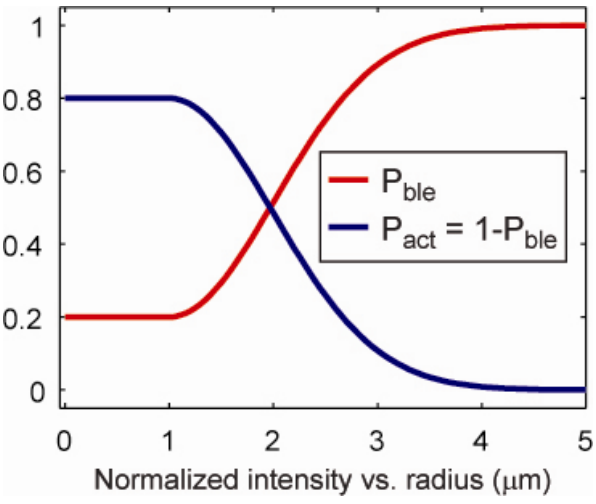

4. Converting from fixed to live cell data

Since GFP's reversible behavior in fixed cells can be different from what is measured in live cells (Fig. S1B), a correction is required to convert the FLAP curve obtained from fixed cell measurements to a corresponding FLAP curve for live cells.

We found that fixation at room temperature yielded the best match between GFP reversible behaviors in fixed and live cells. Under these conditions, the fixed cell recovery curve could be scaled down by a single scale factor to roughly match the live cell recovery curve for a whole nucleus bleach of H2B-GFP indicating fixed cells can replicate the photoswitching behaviors in live cells by introducing the scale factor (Fig. 2D). To see if this held for different reversible fractions, we repeated the whole nucleus bleaches on fixed and live cells using different photobleach intensities. We found that the scale factor from fixed to live cells changed roughly linearly with the size of the reversible fraction (Fig. S4). This calibration curve changed slightly from day to day, presumably due to fluctuations in laser power or small changes in the fixation procedure, so we always performed the calibration on the same day that FRAP curves we collected.

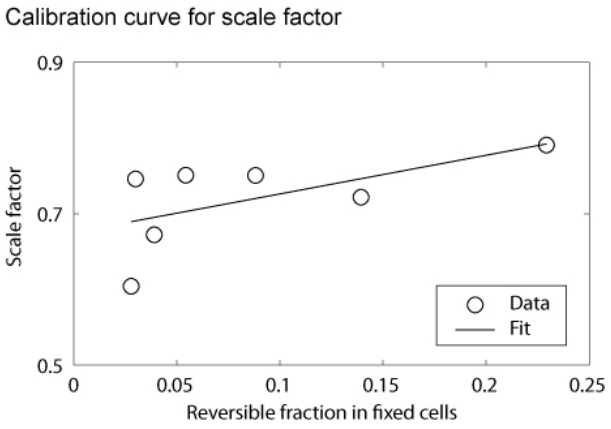

Figure S4. *Converting from fixed to live cell data. The scale factor between live and fixed cell FRAPs varies roughly linearly with the size of the reversible fraction in fixed cells.*

5. Conditions for TBP FRAPs

Table S2 lists the experimental FRAP conditions reported by de Graaf et al. and Chen et al. for their TBP FRAPs, as well as the conditions that we used to approximate these earlier studies (condition #1 for approximating de Graaf et al. and condition #2 for approximating Chen et al.). Not all microscope settings were reported in these earlier studies, and so below we describe how we selected parameters for the unreported settings.

We matched all of the parameter settings reported for the de Graaf et al. TBP FRAP (2). The only settings not explicitly reported were the laser outputs for imaging and bleaching modes, which are difficult to know with certainty unless laser powers are measured at the specimen. To approximate the de Graaf et al. conditions, we set our AOTF and laser outputs such that we detected no observational photobleaching and achieved a bleach depth of 0.27 (Fig. S5A), a situation similar to de Graaf et al. who also detected no observational photobleaching and achieved a bleach depth of 0.29 in U2OS cells.

We also matched all of the reported parameter settings for the Chen el al. TBP FRAP (1), but here a number of key settings were not explicitly described. We attempted to infer these from the images shown and comments made in the paper. The published images show that the whole cell was captured in the field of view, so we set our zoom to 6 which allowed us to do the same. Chen et al. reported that the bleached area was a square with an area of 2 μm^2, so with a zoom of 6 yielding a pixel size of 140 nm at 256x256 pixels resolution, we selected a square bleach 10 pixels on each side to yield a bleached area of ~2 μm^2. The published images show that the bleached region was positioned at different locations along the y axis, depending on the particular experiment. This positioning is important because it determines the time between the bleach and the first image, which will give rise to different reversible fractions. For our condition #2, we positioned this bleached square in the middle of the y axis to account for an average positioning in Chen et al. This middle position for the bleach square yielded a delay time between the bleach and first image of 494 ms. The Chen et al. published data indicate the bleach depth of TBP in HeLa cells was 0.30, and so we adjusted laser outputs, AOTF and scan rate to achieve a bleach depth of 0.29 (Fig. S5B).

In order to measure the “true” bleach depth for proper renormalization of our condition #2 FRAP (Fig.4A), we performed our condition #2 FRAP but with an image size of 256x10 pixels and measured the fluorescent intensity in the bleached region as quickly as possible (with a delay of 21 ms rather than 494 ms). This yielded a “true” bleach depth of 0.13 for condition #2, which was used to renormalize the condition #2 FRAP in Fig. 4B.

Finally, to investigate the effect of expression level of TBP, we performed FRAP in very bright cells using condition #1. Consistent with de Graaf et al. we found that the fast fraction of TBP decreased as TBP levels increased (Fig. S5C).

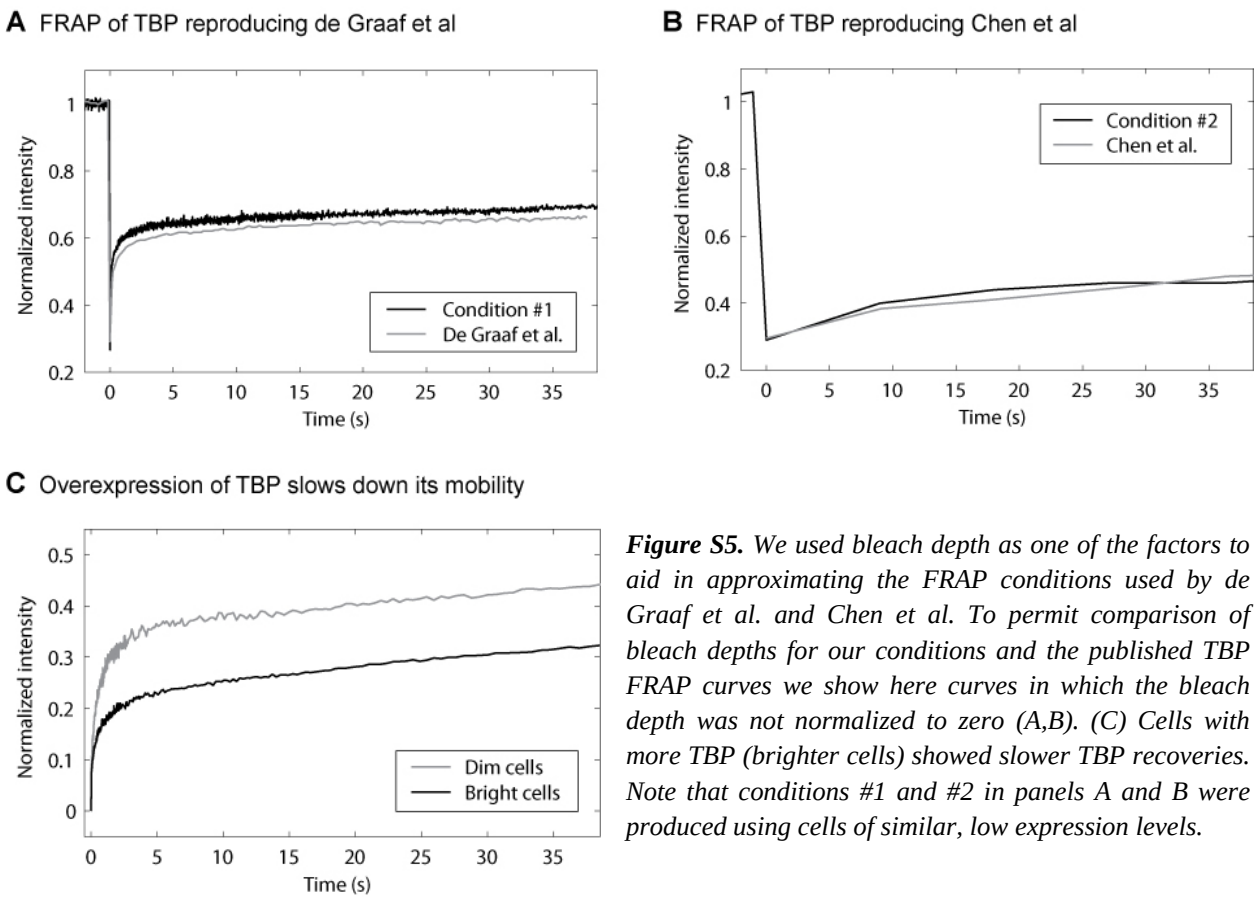

Figure S5. *We used bleach depth as one of the factors to aid in approximating the FRAP conditions used by de Graaf et al. and Chen et al. To permit comparison of bleach depths for our conditions and the published TBP FRAP curves we show here curves in which the bleach depth was not normalized to zero (A,B). (C) Cells with more TBP (brighter cells) showed slower TBP recoveries. Note that conditions #1 and #2 in panels A and B were produced using cells of similar, low expression levels.*

6. Supporting references

1. Chen, D., C. S. Hinkley, R. W. Henry, and S. Huang. 2002. TBP dynamics in living human cells: constitutive association of TBP with mitotic chromosomes. Mol. Biol. Cell. 13: 276-284.

2. De Graaf P., F. Mousson, B. Geverts, E. Scheer, L. Tora, A. B. Houtsmuller, and H. T. Timmers. 2010. Chromatin interaction of TATA-binding protein is dynamically regulated in human cells. J Cell Sci. 123: 2663-2671.

3. Mueller, F., P. Wach, and J. G. McNally. 2008. Evidence for a common mode of transcription factor interaction with chromatin as revealed by improved quantitative fluorescence recovery after photobleaching. Biophysical Journal 94: 3323-3339.

4. Sinnecker, D., P. Voigt, N. Hellwig, and M. Schaefer. 2005. Reversible photobleaching of enhanced green fluorescent proteins. Biochemistry 44: 7085-7094.

5. Sprague, B. L., R. L. Pego, D. A. Stavreva, and J. G. McNally. 2004. Analysis of binding reactions by fluorescence recovery after photobleaching. Biophysical Journal 86: 3473-3495.

7. Supporting tables

Table S1: Microscope settings

Figure	Fig. 1A	Fig. 1B				Fig. 1C	Fig. 1D	Fig. 3
Expressed protein	GFP	YFP	mTFP1	mCherry	TagRFP	H2B-GFP		H2B-GFP
Microscope	Zeiss LSM 5LIVE					Zeiss LSM 5LIVE	Zeiss LSM 510	Zeiss LSM 5LIVE
Laser (nm / mW)	488 / 100		405 / 50	561 / 40		488 / 100	488 / 30	488 / 100
Objective lens	63x/1.4 oil					63x/1.4 oil	40x/1.3 oil	63x/1.4 oil
Laser output (%)	25%		100%			25%	100%	25%
Beam Splitter	BC488					BC488	-	BC488
Dichroic mirror	NFT490			NFT565		NFT490	HFT488	NFT490
Emission filter	LP495			LP580		LP495	505-530	LP495
Pinhole	2.43			2		2.43	2.45	2.43
Detector gain	50.2					50.2	900	50.2
Amplifier offset	0.007					0.007	0	0.007
Amplifier gain	1					1	1	1
Zoom	1					1	6	1
Image size (pixel)	500x500					250x250	10x512	250x250
Image AOTF (%)	6%		3.5%			1%	0.3%	1%
Scan rate (msec/scan)	50					33	21.1 (speed9)	33
Delay (sec)	0					0	0	0
Bleach laser	488 / 100					488 / 100	488 / 30	488 / 100
Bleach laser output	75%					75%	100%	75%
Bleach geometry (pixel)	whole cell (500x500)					whole nucleus (250x250)	strip (10x512)	circle (20)
Bleach AOTF (%)	100%					3% - 100%	100%	5% - 100%
Iterations	1					1	2	1
Laser power (MW/cm^2)	30					1.7 – 30	0.2	2.3 - 30

Table S2: Microscope settings

Figure	Fig. 4A		Fig. 4A,B&C	
Condition	de Graaf et al.	Chen et al.	condition #1	condition #2
Expressed protein	GFP-TBP		TBP/H2B-GFP	
Microscope	Zeiss LSM 510			
Laser (nm / mW)	488 / 200	n.d.	488 / 40	
Objective lens	40x/1.3 oil	n.d.	40x/1.3 oil	
Laser output (%)	n.d.	n.d.	20%	40%
Beam Splitter	-	-	-	
Dichroic mirror	HFT488	n.d.	HFT488	
Emission filter	505-530	n.d.	505-530	
Pinhole	2.48	n.d.	2.45	
Detector gain	900	n.d.	900	
Amplifier offset	0	n.d.	0	
Amplifier gain	1	n.d.	1	
Zoom	6	n.d.	6	
Image size (pixel)	10x512	entire nucleus	10x512	256x256
Image AOTF (%)	n.d.[*1]	n.d.	0.2%	0.3%
Scan rate (msec/scan)	21 (speed9)	n.d.	21.1 (speed9)	987.3 (speed7)
Delay (sec)	0	9	0	9
Bleach laser	488 / 200	n.d.	488 / 30	
Bleach laser output	100%	n.d.	20%	40%
Bleach geometry (pixel)	strip (10x512)	square (2 μm^2)	strip (10x512)	square (10)[*2]
Bleach AOTF (%)	100%	n.d.	45%	90%
Iterations	2	n.d.	2	
Laser power (MW/cm^2)	n.d.	n.d.	1	3.9

*1: They reported that they observed no observational photobleaching.
*2: The bleach square was placed in the middle along the y-axis.
n.d. = not described

Table S3: The magnitude of the reversible fractions under different photobleaching conditions in fixed cells

laser power (MW/cm^2)	30.1	24.2	18.4	12.5	6.7	3.7	2.3
reversible fraction in fixed cells (%) ± SD	9.6 ± 1.4	11.2 ± 0.8	14.5 ± 1.6	16.2 ± 1.2	22.6 ± 0.4	27.6 ± 2.7	37.9 ± 3.7